

Theoretical Analysis of Excited States and Energy Transfer Mechanism in Conjugated Dendrimers

Jing Huang,^[a,b,c] Likai Du,^[a,b,c] Deping Hu,^[a,b,c] and Zhenggang Lan^{*[a,b,c]}

The excited states of the phenylene ethynylene dendrimer are investigated comprehensively by various electronic-structure methods. Several computational methods, including SCS-ADC(2), TDHF, TDDFT with different functionals (B3LYP, BH&HLYP, CAM-B3LYP), and DFT/MRCI, are applied in systematic calculations. The theoretical approach based on the one-electron transition density matrix is used to understand the electronic characters of excited states, particularly the contributions of local excitations and charge-transfer excitations

within all interacting conjugated branches. Furthermore, the potential energy curves of low-lying electronic states as the functions of ethynylene bonds are constructed at different theoretical levels. This work provides us theoretical insights on the intramolecular excited-state energy transfer mechanism of the dendrimers at the state-of-the-art electronic-structure theories. © 2014 Wiley Periodicals, Inc.

DOI: 10.1002/jcc.23778

Introduction

To address the global requirement of renewable energies, the development of novel photovoltaic materials conducting solar energy conversion represents a major challenging task.^[1–4] As a group of promising candidates of photovoltaic compounds, dendrimeric molecules have received wide research interests due to their important photo harvesting and energy transport properties.^[5–7] Such molecules, known for their highly branched tree-like structures, are composed of several linear branches (linear conjugated moieties) linked by meta-substitutions at the phenylene nodes.

One specific type of dendrimer is comprised of phenylene ethynylene (PE) branches, involving 2-ring and 3-ring linear PE units linked by a phenylene node with meta-substitution. The existence of such phenylene node results in the localization of molecular orbitals (MOs) at individual linear PE unit^[8,9] instead of spreading over the whole conjugated systems. Thus, the optically allowed valence electronic excitations generally involve the frontier orbitals within the same units, resulting in the formation of so-called local excited (LE) states. As a result, the absorption spectrum of the whole system simply becomes the summation over the spectrum of each individual chromophore.^[10,11] Different lengths of linear segments result in an energy gradient. When the peripheral groups are initially excited, the exciton is transferred along the branches from the margin to the center of the dendrimer in a unidirectional, multistep manner.^[12–15] Such exciton transfers (energy transfers between different LE excitations) in π -conjugated dendrimers are responsible for the photo-energy collection that can further induce a series of complicated photochemical and photophysical processes.

Numerous efforts were conducted to investigate the excited-state processes of dendrimers, both experimentally^[5,16–18] and theoretically.^[19–22] According to the experimental observations by Shortreed et al.,^[5] the absorption spectra (<400 nm) of dendrimeric systems are barely affected by the addition of ethynyl-

perylene groups while the emission spectra change significantly. The emission from the dendrimeric branches is quenched and fluorescence almost entirely comes from the ethynylperylene group. Additionally, the fluorescence intensity is much higher than that of isolated ethynylperylene systems. This observation obviously proves the existence of the highly-efficient energy funnel associating with the intramolecular excited-state energy transfer from dendrimeric branches to ethynylperylene groups. Swallen et al.^[4] suggested two upper limits of the energy migration timescales, about 10 ps (four-ring unit → core) and 270 ps (periphery → core), according to their measurement of fluorescence lifetime. The further pump-probe spectroscopy experiments by Kleiman et al.^[16] showed the biexponential decay (3.0 ± 0.5 and 14 ± 2.5 ps) for the excited 2-ring branches within the dendrimeric systems, and subpicosecond decays for the 3- and 4-ring units. These experiments successfully confirmed the ultrafast excited-state energy transfer from the shorter PE units to the longer ones. Theoretically, MO calculations by Tada et al.^[23] at the DFT/B3LYP level showed that the MO density is strongly localized in individual chromophores, instead of significant delocalization over the whole conjugated

[a] J. Huang, L. Du, D. Hu, Z. Lan

Key Laboratory of Biobased Materials, Qingdao Institute of Bioenergy and Bioprocess Technology, Chinese Academy of Sciences, Qingdao, 266101 Shandong, People's Republic of China
E-mail: lanzg@qibebt.ac.cn

[b] J. Huang, L. Du, D. Hu, Z. Lan

University of Chinese Academy of Sciences, Beijing 100049, People's Republic of China

[c] J. Huang, L. Du, D. Hu, Z. Lan

The Qingdao Key Lab of Solar Energy Utilization and Energy Storage Technology, Qingdao Institute of Bioenergy and Bioprocess Technology, Chinese Academy of Sciences, Qingdao, 266101 Shandong, People's Republic of China

Contract grant sponsor: CAS 100 Talent Project; Contract grant sponsor: National Natural Science Foundation of China (NSFC); Contract grant numbers: 21103213 and 91233106

© 2014 Wiley Periodicals, Inc.

system. Mukamel, Tretiak, and their coworkers carried out systematic simulations on the exciton transfer of phenylacetylene dendrimers,^[21,24–26] showing the physical insight of exciton coupling and energy-funneling processes. Martínez and coworkers^[27,28] suggested that different branching subunits of the dendrimers are weakly coupled at the ground-state equilibrium geometry while their couplings strongly increase in the excited-state minimum. In this case, the more delocalized excited states should be formed at the emission geometry. In fact, their calculations mainly take the dendrimers with equal-length subunits into account. As pointed out by Palma,^[14] such delocalization may not exist when subunits have different conjugated lengths.

The more comprehensive description of excited-state energy transfer requires the treatment of the nonadiabatic dynamics. Recently, Roitberg and coworkers^[11,29–31] carried out the excited-state nonadiabatic molecular dynamics at the semiempirical AM1/CIS level to study energy transfer within the dendrimer framework. Their work clearly demonstrated that the excited-state energy transfer was governed by the ultrafast nonadiabatic transition between different LE states that were located at different branches. Interestingly, the energy migration was highly unidirectional, namely always from the shorter branching units to the longer ones.^[11,31] For example, the ultrafast energy transfer from the 2-ring to 3-ring unit occurred within 40 fs and the stretching motion of ethynylene bonds in the 2-ring unit was responsible for this ultrafast transfer process.^[11] All these pioneering researches gave us a deep insight of the exciton formation and energy migration in the PE-based materials.

Nevertheless, it is still very important to examine the excited-state characters and analyze energy-transfer mechanism of dendrimers at more precise high-level electronic-structure theory. However, such task is not simple for highly conjugated systems. First of all, the electronic-structure calculations of the molecular excited states represent great challenging.^[32,33] In last decades several high-level methods, such as DFT/MRCI,^[34–40] EOM-CC,^[41–43] CC2,^[44,45] ADC(3),^[46,47] ADC(2),^[48–50] TDDFT^[51,52] were developed to investigate the excited state of middle-sized molecules while the balance between computational cost and accuracy issue is still far from satisfactions. For instance, the widely used TDDFT method often suffers from the wrong description of charge-transfer (CT) states^[32,53,54] that seem to be very critical for organic photovoltaic compounds.^[55,56] The EOM-CC and ADC(3) schemes seem to be very promising due to their accuracy while both of them still suffer from the high computational cost for larger molecule systems. The DFT/MRCI method is also limited to medium molecules,^[38] although it has been recently applied to relatively larger systems, such as thiophene oligomers and fullerene C₆₀.^[37] Second, such organic photovoltaic molecules are generally composed of several building units. A molecular excited state may involve both the LE excitations (Frenkel exciton) and the CT excitations (charge-separated exciton) within interacting units.^[54,57] The analysis of energy transfer processes between different building blocks thus at least requires understanding the contributions of intra-

unit LE and interunit CT transitions. Generally speaking, this analysis protocol is not a trivial task, because excited-state wavefunction may involve several configurations and MOs may be delocalized over several units. To solve this problem, a few pioneering studies have explored the transition density method for detailed analysis of excited-state properties.^[26,31,57–68] Mukamel^[26], Tretiak^[58] and coworkers developed an approach on the basis of the one-electron transition density matrix to analyze the intraunit LE and interunit CT transitions of conjugated molecules. Their methods are mainly based on the semiempirical quantum-chemical calculations that do not take atomic-orbital overlap into account. Recently, Roitberg, Tretiak and their coworkers also introduced this approach into the dynamical simulations and examined the time-dependent transition density to monitor ultrafast energy transfer processes.^[31] Based on the early proposal by Lužanov,^[59,60] Lischka and coworkers proposed an alternative analysis strategy in the basis of the transition density matrix, which can be applied at high-level *ab initio* levels of theories. Their approaches were used to perform the systematic studies on phenylenevinylene oligomer (PV)₆P^[61] and DNA systems.^[62] Recently, Plasser et al.^[63,64] discussed a variety of density matrices-based methods, such as nature difference orbitals, one-electron transition density matrix, state-averaged natural transition orbitals and so on, for the analysis and visualization of the electronic excitations of a diverse set of molecules. By making full use of the locality of the basis in the localized molecular orbital (LMO) representation, an efficient linear-scaling fragments LMO (FLMO)-based TDDFT scheme has been developed by Liu and coworkers^[65]. The FLMOs, which combined the merits of the LMO and canonical molecular orbital representations, are also very useful for the uniform treatment on all kinds of excitations of large systems. The similar sophisticated approach was also suggested by Engels and his coworkers,^[57,67,68] which is useful to perform the character analysis of the excited states for molecular aggregates. Recently, Voityuk^[66] introduced the fragment transition density scheme, with which the diabatic electronic states and their couplings are derived based on the transition density of the adiabatic ones. All these analysis methods are more powerful than previous approaches based on plotting transition densities in cube representation^[53,69] and drawing natural orbitals,^[70] since the contributions of intraunit LE and interunit CT transitions on the excited state can be clearly given in a quantitative manner.

In this article, the small dendrimer composed of 2- and 3-ring linear PE units linked by a phenylene node with meta-substitution was chosen to investigate excited-state properties. We have systematically performed the benchmark calculations for the chosen dendrimer at the SCS-ADC(2), TDDFT (B3LYP, BH&HLYP, CAM-B3LYP), TDHF, and DFT/MRCI levels. The electronic characters of excited states, namely the contributions of the LE and CT excitations, are analyzed by the methods based on transition density matrix. Beside the method by Lischka et al.,^[61,64] another slightly different method^[66] is also used in this article. The potential energy surfaces (PESs) along three ethynylene bonds are computed with above methods. Finally,

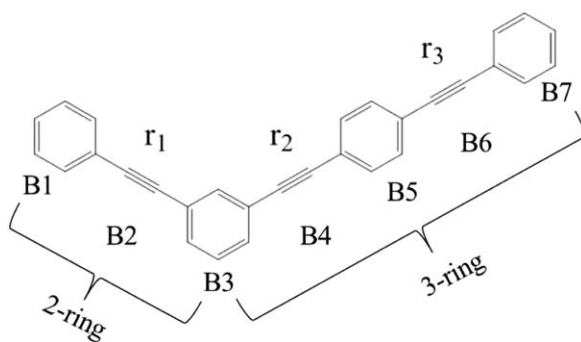


Figure 1. Chemical structure of the chosen molecule that is composed of 2- and 3-ring linear phenylene ethynylene (PE) units linked by meta-substitution at the phenylene node.

through analyzing the PESs and electronic characters of individual excited states, we discuss the contributions of possible energy transfer pathways with different computational methods. The dependence of several frontier orbitals on the key reaction coordinate is examined to get the insight of potential-energy crossings. We expect that this work will help us to examine the unidirectional photoexcitation energy transfer of dendrimers with high-level quantum chemical methods and furthermore provides solid background for nonadiabatic dynamics simulation at more accurate level of theories.

Methods

Model system and labels

This work mainly focuses on the PE dendrimer involving 2-ring and 3-ring linear PE units linked by a phenylene node with meta-substitution (see Fig. 1). The entire molecule is divided into seven blocks (B1–B7) and each functional group is assigned as one block. Three ethynylene bond distances are labeled as r_1 , r_2 , and r_3 in sequence.

As discussed in previous work,^[23] the frontier MOs at the equilibrium geometry are distributed over either 2-ring unit or 3-ring unit (see below orbital analysis). Accordingly, the excited states should involve LE excitations and CT excitations, which are outlined in Scheme 1. In the LE excitations, both initial and final orbitals are located on the same respective fragment, giving $2 \rightarrow 2$ or $3 \rightarrow 3$ LE transitions. The CT excitations, including $2 \rightarrow 3$ and $3 \rightarrow 2$ excitations, denote that the initial and final orbitals are located on different fragments. When the molecular geometry is beyond the equilibrium structure, the MOs may show remarkable different shapes (see below discussions). Some of orbitals may spread over not only 2-ring unit but also 3-ring unit. In this case, we refer the orbitals locating

Table 1. Electronic characters of different electronic transitions

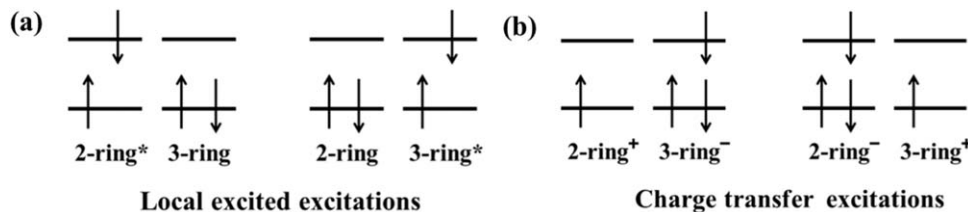
Electronic transition ^[a]	Electronic character ^[b]
$2 \rightarrow 2$	LE1
$2 \rightarrow 3$ and (or) $3 \rightarrow 2$	CT1
$3 \rightarrow 3$	LE2
$4 \rightarrow 4$	LE3
$4 \rightarrow 3/2$ and (or) $3/2 \rightarrow 4$	CT2

[a] $m \rightarrow n$: m and n refer to the locations of orbitals involved in electronic transitions. [b] In the LE excitations, both initial and final orbitals are located on the same fragment. The CT excitations denote that the initial and final orbitals are located on different fragments.

in the “4-ring” unit instead. Then, the excited state may involve other configurations, such as local $4 \rightarrow 4$ transitions, as well as CT transitions from the 4-ring to the 3-ring/2-ring and vice versa. Table 1 gives the notation of possible electronic transitions, such as $2 \rightarrow 2$, $2 \rightarrow 3$ and (or) $3 \rightarrow 2$, $3 \rightarrow 3$, $4 \rightarrow 4$, $4 \rightarrow 3/2$, and (or) $3/2 \rightarrow 4$. Shortly, we always used “ $m \rightarrow n$ ” to label the LE or CT excitation, where m and n refer to the location of orbitals involved in electronic transitions. To avoid confusing, in the discussion of the energy transfer, a long expression “ m -ring \rightarrow n -ring” denotes the excited-state energy transfer from the m -ring unit to the n -ring unit, corresponding to the transitions from $m \rightarrow m$ LE state to $n \rightarrow n$ LE state.

Electronic-structure theories

Several electronic-structure methods, such as SCS-ADC(2),^[71] DFT/TDDFT,^[72–75] HF/TDHF,^[76] and DFT/MRCI,^[34–40] were used to treat the excited states. The selection of functionals is very critical in the DFT/TDDFT treatments.^[37,54,77] The pure functionals were not taken here because they could strongly underestimate the energy of CT states.^[54] It is also well known that the energy of CT excitation is highly influenced by the percentage of HF exchange for hybrid functional.^[53,54] Therefore, several functionals such as B3LYP^[78–83] (20% HF), BH&HLYP^[78–80] (50% HF), and CAM-B3LYP^[84] (long-range corrected) were used for benchmark reasons. As reported by many previous studies,^[32,53,54] TDDFT approaches tend to underestimate the energy of CT excitation whereas the opposite holds true for TDHF.^[54] Therefore, TDHF was also considered in this benchmark work. The CT states seem not a serious issue within the ADC(2) approach,^[62] which is thus commonly thought to be a rather accurate method. Here, to increase the robustness of ADC(2) against strong correlation effects, in particular for systems with triple bonds,^[85] its spin-component scaling modification SCS-ADC(2)^[71] was applied in the current work. Such spin-component scaling approach also



Scheme 1. Excitation scheme for electronically local excited (LE) excitations a) and charge-transfer (CT) excitations b).

systematically enhances the accuracy for 0–0 excitation energies for $\pi-\pi^*$ transitions.^[85] Similarly, Engels and coworkers also recommended the employment of SCS-CC2 in excited-state calculations.^[54,57] Recently, the weights of doubly excited configurations are suggested to be important with increasing the chain length of the linear polyenes by Dreuw et al.^[86] To properly describe states with double excitation character, the DFT/MRCI method^[34–40] was also used, which in principle provides the reasonable description of both valence and CT excited states for organic systems. The initial reference configurations were generated from up to two (active) electrons out of 10 electrons in 10 active orbitals. Originally, Grimme and Waletzke^[34] reported that the calculated energies of the electronic states depend on the choice of the configuration selection threshold (δE_{sel}). Here, the effects of different values of δE_{sel} were investigated, shown in Figure S1 in Supporting Information (SI). For $\delta E_{\text{sel}} \leq 1.0$, the deviations of the calculated excitation energies are less than 0.15 eV and most importantly the order of low-lying excited states remains identical. In consideration of the accuracy and affordable computation time, we used $\delta E_{\text{sel}} = 0.9$ for all DFT/MRCI calculations.

In this work, SCS-ADC(2)/TZVP, B3LYP/TZVP, BH&HLYP/TZVP, and TDHF/TZVP calculations were carried out with the Turbomole 6.3^[87] program while the CAM-B3LYP/6-311G* calculation was performed with the Gaussian09^[88] program. The DFT/MRCI calculation was done with the MRCI code by Grimme and Waletzke,^[34] which is linked to Turbomole. The potential energy curves of several low-lying excited states were obtained as functions of the ethynylene bond distances r_1 , r_2 , and r_3 .

Electronic character analysis

As discussed before, electronically excited states may involve different LE or CT components. It should be interesting to analyze the excited-state characters and all possible excitations (LE or CT) to gain a useful insight into the excited states of the PE dendrimer. First, the protocol by Lischka and Plasser^[61] was considered for this purpose. The one-electron transition density matrix is defined as

$$T_{rs}^{\text{EG}} = \langle E | a_r^\dagger a_s | G \rangle \quad (1)$$

Here, T_{rs}^{EG} defines the transition density between MOs s and r . $|E\rangle$ ($|G\rangle$) refers to the excited (ground) state many-electron wave function. a_r^\dagger (a_s) is the creation (annihilation) operator for an electron at the r th (s th) MO. The transformation of transition density matrix from the MO basis to the atomic orbital (AO) basis is performed as follows:

$$T^{[\text{AO}]} = C T^{[\text{MO}]} C^t \quad (2)$$

where $T^{[\text{AO}]}$ is the one-electron density matrix in the AO basis, C is the MO coefficient matrix. The AO overlap matrix is given by

$$S^{[\text{AO}]} = C^{-1,t} S^{[\text{MO}]} C^{-1} = C^{-1,t} C^{-1} \quad (3)$$

where the MO overlap matrix $S^{[\text{MO}]}$ is the unit matrix. For an excited state, the total transition probability between two

atoms in principle should be given by simply adding all relevant AO transitions. However, the AO basis is nonorthogonal and thus the AO overlap matrix should be taken into account. The total transition probability from one atom to another is defined as eq. (4), a somewhat altered form was also given in recent published reference.^[64]

$$B_{ab}^E = \sum_{\substack{r \in a \\ s \in b}} \left(T^{\text{EG},[\text{AO}]} \right)_{rs} \left(S^{[\text{AO}]} T^{\text{EG},[\text{AO}]} \right)_{rs} \quad (4)$$

Lischka and coworkers^[61] once pointed out that this approach is in analogy to Mayer's bond order^[89] between two atoms, a and b . In the below discussion, this method is defined as Lischka's approach.

Alternatively, another similar analysis by projecting the term $T^{\text{EG},[\text{AO}]}$ into the Löwdin orbitals as displayed in eq. (5).^[66]

$$T^{\text{EG},[\text{Lo}]} = (S^{[\text{AO}]})^{\frac{1}{2}} T^{\text{EG},[\text{AO}]} (S^{[\text{AO}]})^{\frac{1}{2}} \quad (5)$$

where the transition density matrix $T^{\text{EG},[\text{Lo}]}$ is formed in the orthogonal Löwdin orbital basis.^[90] In this sense, the transition probability from one atom to another can be simply expressed as eq. (6).

$$B_{ab}^E = \sum_{\substack{r \in a \\ s \in b}} \left(T^{\text{EG},[\text{Lo}]} \right)_{rs} \quad (6)$$

Similarly, we defined this method as the method based on the Löwdin orbital basis. Let us consider two fragments A and B in a molecule. Regardless of using Lischka's approach or the method based on the Löwdin orbital basis, the transition probability from fragment A to fragment B can be obtained by summing B_{ab}^E as shown in eq. (7).

$$\Omega_{AB}^{\text{EG}} = \sum_{\substack{a \in A \\ b \in B}} B_{ab}^E \quad (7)$$

If $A \neq B$, eq. (7) represents the CT probability from A to B , whereas it refers to the LE transition if $A = B$. In this way, we can easily view all intraunit LE and interunit CT contributions for an excited state. Engels and his coworkers also used the analogy efforts to build the transition density in orthogonalized bases while they used localized MOs that need to be built explicitly.^[57,67,68]

In the analysis based on the SCS-ADC(2) and DFT/MRCI calculations, the singly excited amplitudes were chosen to represent the single-electron excitations. This treatment should be reasonable if an excited-state wave function is dominant by single excitations.^[61,62]

Results and Discussion

Vertical excitation energies and electronic characters of excited states at equilibrium geometry

SCS-ADC(2)/TZVP level. Usually, the electronic characters of excited states are determined by MOs involved in electronic

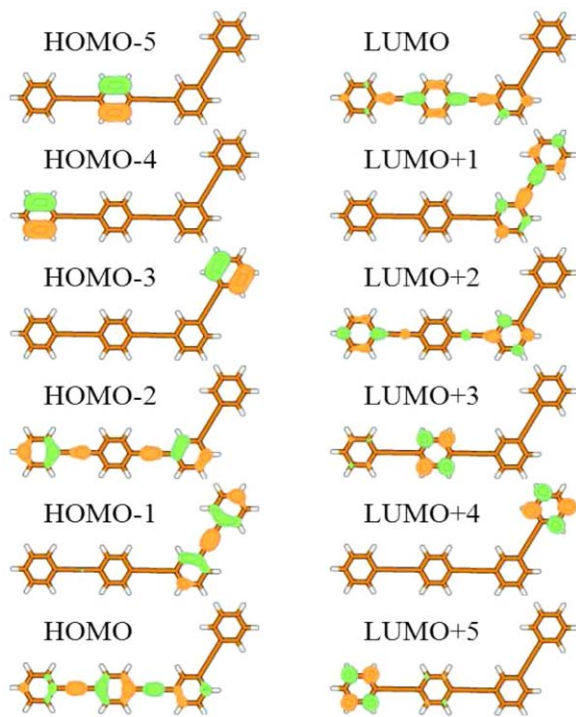


Figure 2. MOs (SCS-ADC(2) level) of the studied molecule at the optimized ground-state geometry. [Color figure can be viewed in the online issue, which is available at wileyonlinelibrary.com.]

excitations. Several frontier π MOs at the SCS-ADC(2)/TZVP level are shown in Figure 2. At the ground-state equilibrium geometry, all frontier orbitals are located at either 3-ring unit or 2-ring unit. Among them, HOMO-5, HOMO-4, HOMO-2, HOMO, LUMO, LUMO+2, LUMO+3, and LUMO+5 are localized at the 3-ring unit while the HOMO-3, HOMO-1, LUMO+1, and LUMO+4 are localized at the 2-ring unit. We notice that all DFT methods with different functionals give similar frontier MOs at their own optimized equilibrium geometries, thus only the orbitals obtained at the SCS-ADC(2) level are shown here and the orbitals at other levels of theory are given in SI (Figure S2-S5).

Several low-lying excited states at the ground-state minimum geometry are obtained at the SCS-ADC(2)/TZVP level (Table 2). All six lowest excited states (S_1 – S_6) belong to A' symmetry. The contributions of double excitations to each excited state (approximately 10%) are listed in Table S1 (SI), exhibiting dominant single excitation character. From Table 2, the bright S_1 state with large oscillator strength is dominated by one major HOMO \rightarrow LUMO transition. Since both HOMO and LUMO are located in the 3-ring unit (Fig. 2), S_1 represents a typical $3 \rightarrow 3$ LE state. The S_2 state is essentially dark due to much smaller oscillator strength. The major transitions of S_2 are highly mixed, involving several transitions from different orbitals locating between HOMO-2 and LUMO+2. Interestingly, S_2 includes both $2 \rightarrow 3$ CT transitions and reversed $3 \rightarrow 2$ CT transitions. In this sense, both two (2-ring and 3-ring) units behave as electron donor and accepter at the same time. All S_3 , S_4 , and S_5 are dark with small oscillator strengths while the former two states (S_3 and S_4) mainly include the $3 \rightarrow 3$ LE

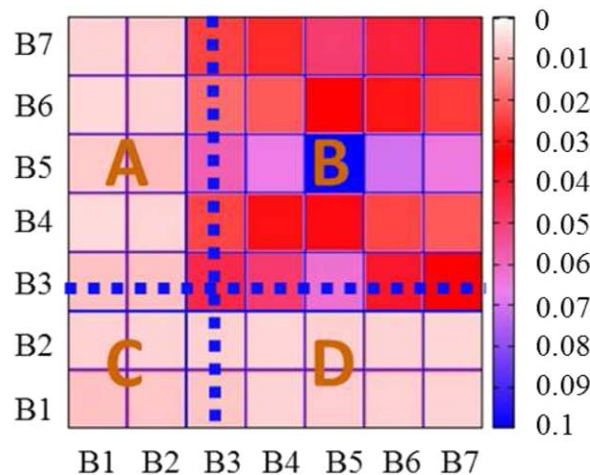
Table 2. Vertical excitation energies (ΔE , eV), oscillator strengths (f), and dominant contributions (Dom. Contr.) of excited states at the SCS-ADC(2)/TZVP level.^[a]

State	ΔE (eV)	f	Dom. Contr.	Label
S_1	4.325	2.624	HOMO \rightarrow LUMO(80%)	$3 \rightarrow 3$
	4.463	0.001	HOMO-1 \rightarrow LUMO(15%)	$2 \rightarrow 3$
S_2			HOMO \rightarrow LUMO+1(12%)	$3 \rightarrow 2$
			HOMO-1 \rightarrow LUMO+2(12%)	$2 \rightarrow 3$
S_3	4.579	0.000	HOMO-5 \rightarrow LUMO(38%)	$3 \rightarrow 3$
			HOMO \rightarrow LUMO+3(34%)	$3 \rightarrow 3$
S_4	4.803	0.000	HOMO-4 \rightarrow LUMO+2(19%)	$3 \rightarrow 3$
			HOMO-4 \rightarrow LUMO(18%)	$3 \rightarrow 3$
S_5	4.814	0.001	HOMO-3 \rightarrow LUMO+1(32%)	$2 \rightarrow 2$
			HOMO-1 \rightarrow LUMO+4(30%)	$2 \rightarrow 2$
S_6	4.909	1.048	HOMO-1 \rightarrow LUMO+1(61%)	$2 \rightarrow 2$
			HOMO \rightarrow LUMO+1(13%)	$3 \rightarrow 2$
			HOMO-1 \rightarrow LUMO(12%)	$2 \rightarrow 3$

[a] Only the components with the contribution more than 10% are included.

transitions and the latter one (S_5) becomes a $2 \rightarrow 2$ LE state. Additionally, the energies of S_4 and S_5 resemble with each other, indicating the possible existence of the S_4/S_5 PES crossing at the Frank-Condon (FC) region. The S_6 state with the high oscillator strength dominantly includes the HOMO-1 \rightarrow LUMO+1 transition. Although this state could mainly be assigned as a $2 \rightarrow 2$ LE state responsible for the strong absorption of 2-ring unit, the CT ($2 \rightarrow 3$ and $3 \rightarrow 2$) excitations are also involved.

To determine the electronic characters of excited states more directly, the transition density analysis of each state is performed based on both Lischka's approach and the method



Scheme 2. The classification of electronic transition within all seven (B_1 – B_7) blocks. Each square stands for the transition from the B_x (horizontal) to B_y (longitudinal) blocks. The whole plot is divided by the bold blue dash line, giving four parts representing different transitions [A) $2 \rightarrow 3$ CT, B) $3 \rightarrow 3$ LE, C) $2 \rightarrow 2$ LE, and D) $3 \rightarrow 2$ CT]. The color codes in this figure, as well as in the remaining figures of this article, indicate the amplitude of transition probability. [Color figure can be viewed in the online issue, which is available at wileyonlinelibrary.com.]

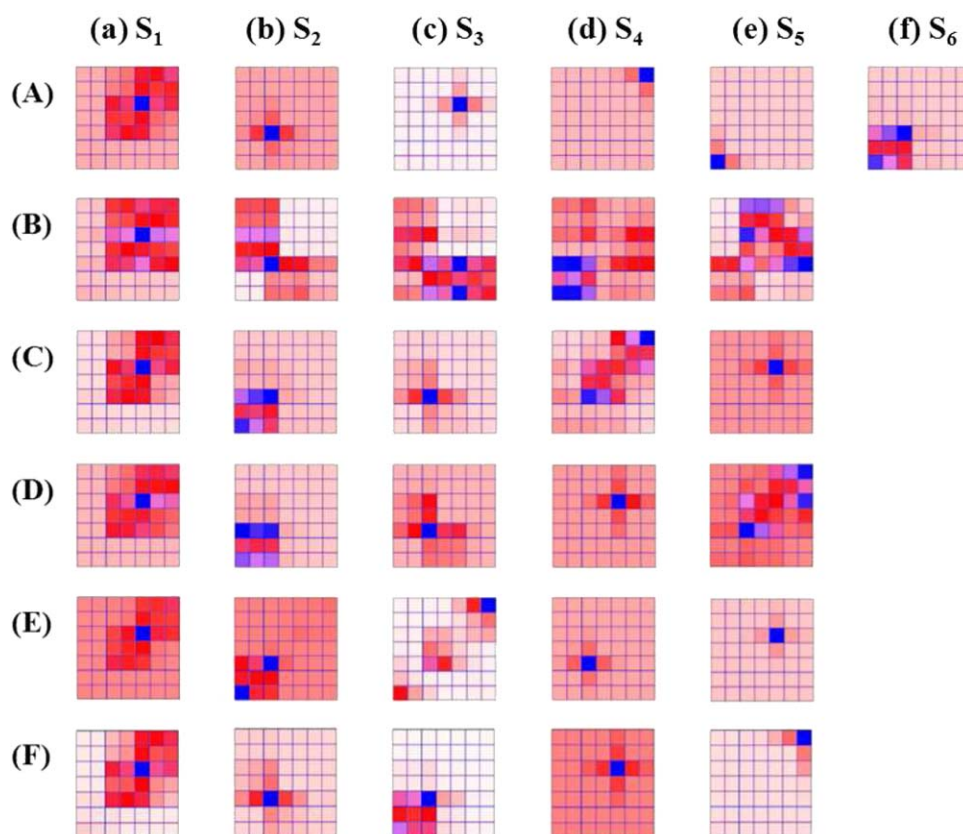


Figure 3. The transition density analysis for the low-lying singlet excited states (a–f) with the method based on the Löwdin orbital basis at the A) SCS-ADC(2)/TZVP, B) B3LYP/TZVP, C) BH&HLYP/TZVP, D) CAM-B3LYP/6-311G*, E) TDHF/TZVP, and F) DFT/MRCI levels. Although at the SCS-ADC(2)/TZVP level the S_5 state corresponds to the lowest $2 \rightarrow 2$ transition, it is essentially dark. As the contrast, the S_6 state is responsible for the first bright $2 \rightarrow 2$ excitation. For other levels, the lowest $2 \rightarrow 2$ transition results in the bright excited state.

based on the Löwdin orbital basis. As displayed in Scheme 2, seven blocks (B1–B7 in Fig. 1) are used to build intraunit and interunit transition probabilities. Every square in Scheme 2 represents the transition from the corresponding horizontal block (horizontal axis) to the longitudinal block (longitudinal axis). In each square, the deeper color represents the larger transition. Furthermore, the 7×7 array panel is split into four parts: (A) $2 \rightarrow 3$ CT, (B) $3 \rightarrow 3$ LE, (C) $2 \rightarrow 2$ LE, and (D) $3 \rightarrow 2$ CT. The diagonal length represents the local excitation on 2-ring or 3-ring, whereas the off-diagonal elements correspond to CT configurations.

Figure 3A provides the transition density analysis for six excited states at the SCS-ADC(2)/TZVP level. Due to the similar results obtained by Lischka's approach [eq. (4)] with the corresponding outcomes of the method based on the Löwdin orbital basis [eq. (6)], in below discussions we only present the results based on the latter approach and put the data obtained by Lischka's approach in SI (Figure S6–S10). It is clear that the S_1 state is a $3 \rightarrow 3$ LE state (Fig. 3Aa), consistent to its dominant electronic configuration in Table 2. Previous analysis has figured out that the S_2 state is a CT state including both $2 \rightarrow 3$ and $3 \rightarrow 2$ CT excitations. Here, we find more insight on which block is directly related to such transitions. Figure 3Ab shows that the electronic transition of S_2 state mainly occurs at the B3 block, namely the core block belonging to not only the 2-ring unit but also the 3-ring unit. The

electronic transition from B3 to itself becomes an important component for the S_2 state. The CT ($2 \rightarrow 3$ and $3 \rightarrow 2$) excitations (assigned by involved orbitals) should mainly involve the transitions either from B3 to adjacent block or vice versa. In this sense, this analysis provides more insight on electronic excitations than the standard orbital picture. Particularly when the electronic transition involves too many orbitals, it is very difficult to obtain all transition components from the standard orbital analysis while this approach becomes more powerful. Both S_3 and S_4 are $3 \rightarrow 3$ LE states and their components are mainly characterized by the transitions at the benzene block (B5 and B7, respectively), as shown in Figure 3Ac and Figure 3Ad, respectively. Although the S_5 state is the first state of the $2 \rightarrow 2$ LE transition (Figure 3Ae), it is essentially dark. The first bright state attributed to the $2 \rightarrow 2$ LE transition is the S_6 state (Fig. 3Af) while it contains weak CT excitation. Hence, at the SCS-ADC(2) level, the photoinduced energy transfer (2-ring \rightarrow 3-ring) seems to involve a rather complex process and many excited states, since the initial $2 \rightarrow 2$ optically allowed excitation gives the S_6 state.

B3LYP/TZVP level. At the TDDFT level with B3LYP functional and TZVP basis, the vertical excitation energies, oscillator strengths, and dominant contributions of excited states are listed in Table S2 in SI. The corresponding transition density analysis is shown in Figure 3B. Similar to SCS-ADC(2), Figure 3B

Table 3. Vertical excitation energies (ΔE , eV), oscillator strengths (f), and dominant contributions (Dom. Contr.) of excited states at the BH&HLYP/TZVP level.^[a]

State	ΔE (eV)	f	Dom. Contr.	Label
S_1	3.945	2.189	HOMO → LUMO(84%)	$3 \rightarrow 3$
S_2	4.538	0.821	HOMO-1 → LUMO+1(57%)	$2 \rightarrow 2$
			HOMO-1 → LUMO(18%)	$2 \rightarrow 3$
			HOMO → LUMO+1(12%)	$3 \rightarrow 2$
S_3	4.684	0.007	HOMO → LUMO+1(29%)	$3 \rightarrow 2$
			HOMO-1 → LUMO(28%)	$2 \rightarrow 3$
			HOMO-1 → LUMO+2(10%)	$2 \rightarrow 3$
S_4	4.962	0.0497	HOMO-2 → LUMO(43%)	$3 \rightarrow 3$
			HOMO → LUMO+2(21%)	$3 \rightarrow 3$
			HOMO-1 → LUMO+1(10%)	$2 \rightarrow 2$
S_5	4.999	0.000	HOMO → LUMO+3(47%)	$3 \rightarrow 3$
			HOMO-5 → LUMO(37%)	$3 \rightarrow 3$

[a] Only the components with the contribution more than 10% are included.

shows that the S_1 state is also assigned as the $3 \rightarrow 3$ LE state. Although both the SCS-ADC(2) and TDDFT/B3LYP calculations give the CT character for the S_2 state, significant differences exist between two sets of results. At the SCS-ADC(2) level, many configurations contribute to the S_2 excited state wave functions while only two configurations play a dominant role at the TDDFT/B3LYP level. In addition, the CT excitation either starts from or ends up with B3 block at the SCS-ADC(2) level, (Fig. 3Ab), while it involves almost all blocks in the 2-ring and 3-ring fragments at the TDDFT/B3LYP level (Fig. 3Bb). In another word, the long-range delocalized CT excitation is more favorable at the TDDFT/B3LYP level. The S_3 state is also a CT state including both $2 \rightarrow 3$ and $3 \rightarrow 2$ CT transitions (Fig. 3Bc). Both the orbital and transition density analysis show that the bright S_4 state is mainly composed of the $2 \rightarrow 2$ LE transition, responsible for the photoabsorption of the 2-ring unit (Fig. 3Bd). The S_5 state is assigned as the $3 \rightarrow 3$ LE state (Fig. 3Be), while its energy is similar to that of S_4 .

BH&HLYP/TZVP and CAM-B3LYP/6-311G* levels. With the introduction of more HF exchanges, the BH&HLYP/TZVP calculations give another view (Table 3). Similar to both SCS-ADC(2) and TDDFT/B3LYP, the TDDFT/BH&HLYP predicts that S_1 is the bright $3 \rightarrow 3$ LE state (Fig. 3Ca) with the HOMO → LUMO transition. However, significant differences are obtained for higher excited states. The S_2 is another bright state with three major transitions, including one leading $2 \rightarrow 2$ LE transition and two minor CT ($2 \rightarrow 3$ and $3 \rightarrow 2$) transitions (Table 3). Considering its oscillator strength and the transition density distribution (Fig. 3Cb), S_2 can be safely assigned as the $2 \rightarrow 2$ LE state responsible for the photoabsorption of the 2-ring unit. The other states (S_3 , S_4 , and S_5) carry weaker oscillator strengths, belonging to the dark states. Essentially S_3 is a CT state while S_4 and S_5 are $3 \rightarrow 3$ LE states with very similar energy. More details are summarized in Table 3 and Figure 3Cc–3Ce. At the TDDFT/BH&HLYP level, we did not find CT state between the bright $3 \rightarrow 3$ and $2 \rightarrow 2$ LE states. As a result, the more simple process involving direct 2-ring → 3-ring energy transfer is implied after the excitation of the 2-ring unit. Most likely the CT state should not be involved in the energy funnel process

at all. In comparison with TDDFT/B3LYP (20% HF), TDDFT/BH&HLYP (50% HF) predicts much higher vertical excitation energies for not only CT states but also LE states. Similar observations have also been found in some other systems.^[38,77] Certainly, the CT states shift to the higher energy domain while the components of the CT states are also strongly influenced by the HF exchange. The lowest CT state (S_3) at the TDDFT/BH&HLYP displays the shorter-distance CT excitations between the B3 block and its adjacent ones, see Figure 3Cc. Similar to results at SCS-ADC(2) level, the more local CT excitations are involved.

The CAM-B3LYP/6-311G* method gives the essentially consistent results with BH&HLYP/TZVP, particularly for the lowest three excited states (Table S3 in SI and Fig. 3D). Only slight minor differences on the interunit excitations have been observed, possibly due to different HF exchange. The order of high-lying states (S_4 and S_5) seems to be reversed while their energies are very similar. Thus, their energy order and electronic characters show the strong dependence on computational methods.

TDHF/TZVP level. At the TDHF/TZVP level (Table S4 and Fig. 3E), the overall electronic characters of first two excited states (S_1 and S_2) resemble their counterparts at BH&HLYP level. Thus, the S_1 and S_2 are safely assigned as $3 \rightarrow 3$ and $2 \rightarrow 2$ LE states, respectively (Figs. 3Ea and 3Eb). It is well known that the excitation energies of excited states in general shift to the high energy domain at the TDHF level and this situation becomes even more significant for the CT states.^[54] This feature is observed in these calculations, see Table 4 and Figure 3E. However, the TDHF and TDDFT/BH&HLYP levels predict the similar excited-state energy-transfer mechanism.

DFT/MRCI level. Figure 3F provides the transition density analysis for five lowest excited states at the DFT/MRCI level. The corresponding major orbital transitions are shown in Table 4. Similar to other methods, the DFT/MRCI predicts that S_1 is the $3 \rightarrow 3$ LE state (Fig. 3Fa), which is dominated by the HOMO → LUMO transition. Owing to the two major transitions, including HOMO-1 → LUMO and HOMO → LUMO+1, S_2 is characterized

Table 4. Vertical excitation energies (ΔE , eV), single excitation, double excitation, and dominant contributions (Dom. Contr.) of excited states at the DFT/MRCI level.^[a]

State	ΔE (eV)	Dom. Contr.	Label
S_1	3.419	HOMO → LUMO(73%)	$3 \rightarrow 3$
S_2	3.704	HOMO-1 → LUMO(26%)	$2 \rightarrow 3$
		HOMO → LUMO+1(18%)	$3 \rightarrow 2$
S_3	3.942	HOMO-1 → LUMO+1(46%)	$2 \rightarrow 2$
		HOMO → LUMO+1(18%)	$3 \rightarrow 2$
		HOMO-1 → LUMO (13%)	$2 \rightarrow 3$
S_4	4.056	HOMO-5 → LUMO (35%)	$3 \rightarrow 3$
		HOMO → LUMO+3(34%)	$3 \rightarrow 3$
S_5	4.184	HOMO-4 → LUMO (23%)	$3 \rightarrow 3$
		HOMO → LUMO+4(18%)	$3 \rightarrow 2$
		HOMO-4 → LUMO+2(14%)	$3 \rightarrow 3$
		HOMO-2 → LUMO+4(11%)	$3 \rightarrow 2$

[a] Only the components with the contribution more than 10% are included.

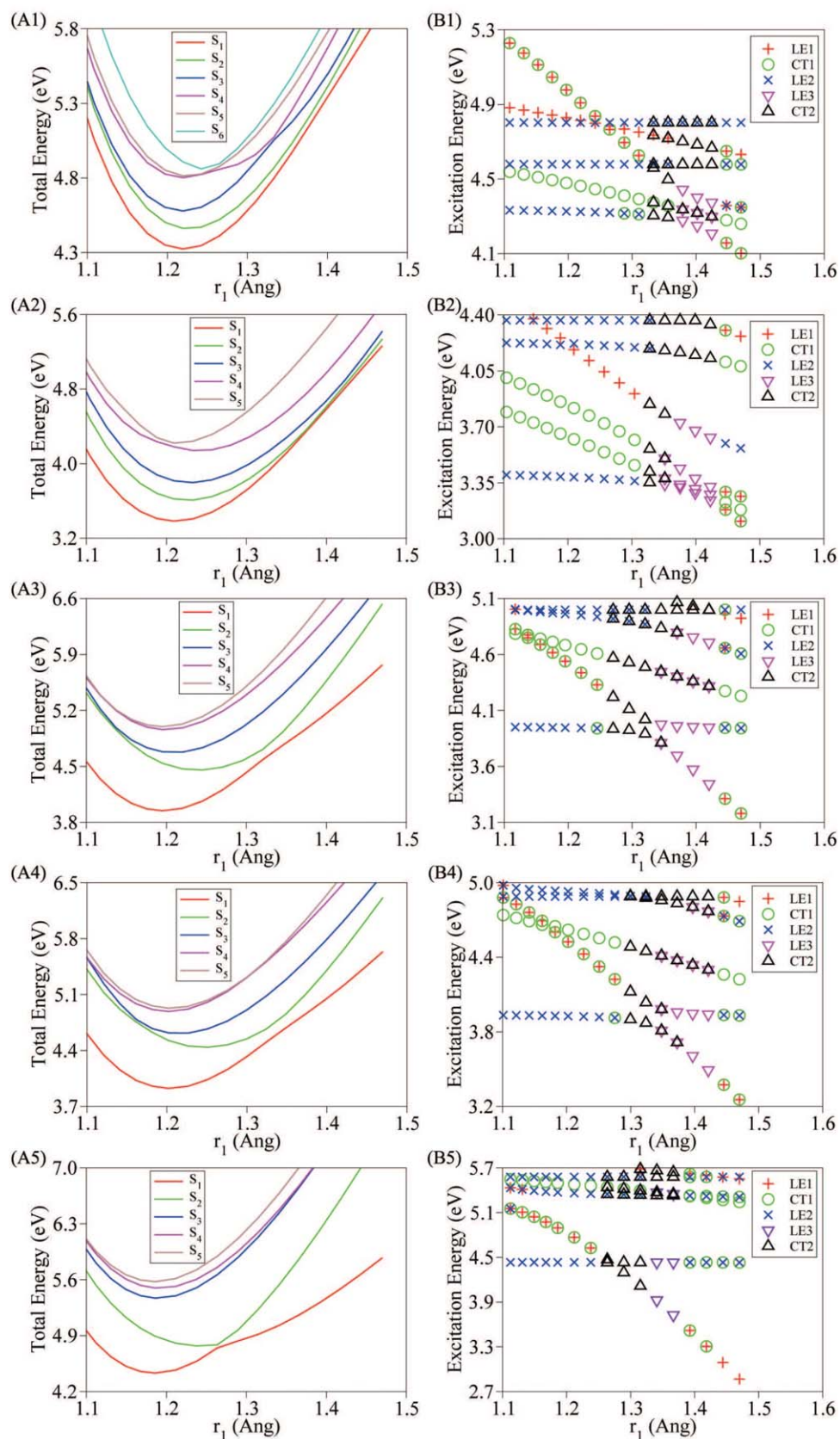


Figure 4. The results at different levels: A1-B1) SCS-ADC(2)/TZVP; A2-B2) B3LYP/TZVP; A3-B3) BH&HLYP/TZVP; A4-B4) CAM-B3LYP/6-311G*, and A5-B5) TDHF/TZVP levels. The left column A1-A5) gives the PESs (S_1 : red, S_2 : green, S_3 : blue, S_4 : magenta, S_5 : brown, S_6 : turquoise). The right column B1-B5) shows the dependence of all electronic transitions on r_1 and excitation energies (LE1: plus, CT1: circle, LE2: x, LE3: triangle down, CT2: triangle up). [Color figure can be viewed in the online issue, which is available at wileyonlinelibrary.com.]

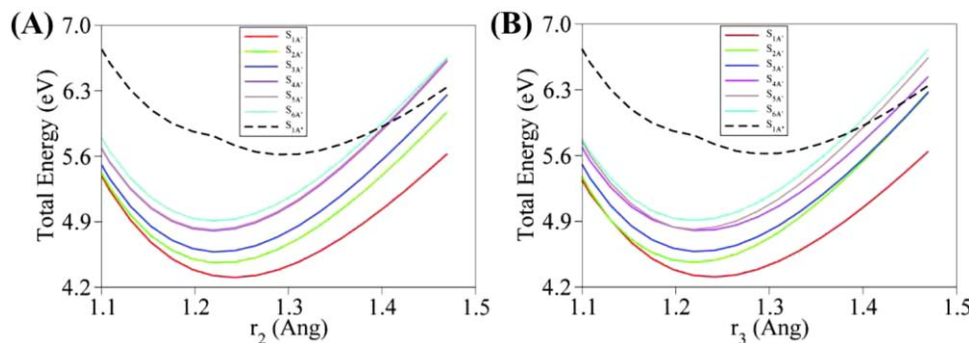


Figure 5. The PES (SCS-ADC(2)/TZVP) as the function of A) r_2 and B) r_3 . (The solid line and dashed line indicate the excited state with symmetry A' and A'' , respectively. S_{1A}' : red, S_{2A}' : green, S_{3A}' : blue, S_{4A}' : magenta, S_{5A}' : brown, S_{6A}' : turquoise, S_{1A}'' : black). [Color figure can be viewed in the online issue, which is available at wileyonlinelibrary.com.]

as the CT state (Fig. 3Fb). The first $2 \rightarrow 2$ LE state appears at S_3 (Fig. 3Fc) and some CT components are also involved. Significantly, compared with Figure 3C (TDDFT/BH&HLYP), the order of S_2 and S_3 seems to be reversed, that is, the CT state was pulled down at DFT/MRCI level. Here, to give an overall comparison more clearly, the contributions of different transitions ($2 \rightarrow 2$, $3 \rightarrow 3$, $2 \rightarrow 3$, and/or $3 \rightarrow 2$) to the lowest states based on different levels at the equilibrium geometry are also given by some numerical representations (Figure S11 in SI). To be more specific, the double excitation contributes to the five lowest excited states is less than 10% (Table S5). Considering the little double excitation contributions to each studied excited state at DFT/MRCI as well as SCS-ADC(2) level, the excited states of the PE dendrimer do not possess significant double excitation character.

PES and electronic characters of excited states at different computational levels

Previous studies by Roitberg and coworkers^[11] have shown that the ethynylene bond r_1 (2-ring unit), instead of r_2 and r_3 (3-ring unit), is the main reaction coordinate responsible for the energy transfer process of PE compound. Thus, we explore the PESs and their crossings along all three ethynylene bond distances at the high levels of electronic-structure theories. This result also suggests that the stretching motions of r_2 and r_3 are not the major reaction coordinates because of the high energies of their relevant PES crossings. At the same time, we notice that all low-lying electronic states are of A' symmetry at all levels. It is highly possible that the A'' states are not involved in the excited-state energy transfer, because the PES crossings between the A'' state and A' state lie in the higher energy area. Although at some theoretical level (such as TDHF), the energies of the A'' states become lower with the elongations of the bond distance, their crossings with the A' state are still higher than the reactive pathways (see SI, Figure S12). Therefore, in this section, we mainly discuss the PESs of excited states of the A' symmetry along the r_1 coordinates and put others into the SI. For the better view of crossings and electronic characters, both PESs and excitation energies are plotted as the functions of r_1 (Fig. 4).

At the SCS-ADC(2) level of theory (Fig. 4A1), the excited-state energy transfer mechanism seems to be very complex,

which involves several excited states. The photoexcitation prepares a bright $2 \rightarrow 2$ LE state (S_6) with a high energy. Immediately after it, the bond stretching along r_1 brings the system accessing the S_5/S_6 conical intersections (or avoided crossings), where nonadiabatic transitions take place. Then, this vibrational motion along r_1 further takes the system into the area with very long r_1 distance ($r_1 > 1.33$ Ang). In this region, the frontier MOs become delocalized over the whole systems and thus the $4 \rightarrow 4$ excitations appear. Such orbital variation causes the strong electronic couplings between different excited states. This induces the further nonadiabatic decay and the system may finally reach the lowest $3 \rightarrow 3$ LE excited state. Overall, the SCS-ADC(2) suggests a complex energy transfer funnel, since a few of intermediate states are involved.

At the TDDFT/B3LYP level, a conical intersection exists between S_4 and S_5 state at the FC region (Fig. 4A2), which is the crossing between the bright $2 \rightarrow 2$ LE state and the dark $3 \rightarrow 3$ LE state. Here, two CT states lie between the bright $2 \rightarrow 2$ LE state and the lowest $3 \rightarrow 3$ LE state. The strong mixing and delocalization of frontier orbitals were also observed at longer r_1 distances. As a result, the crossing between CT states and the lowest bright $3 \rightarrow 3$ LE state is formed. However, it is not possible to derive the energy transfer mechanism at the TDDFT/B3LYP level only according to the PES along r_1 . This implies that other degrees of freedom must play an essential role at such level of theory.

Interestingly, the similar PES profiles of low-lying excited states are obtained at the BH&HLYP/TZVP (Fig. 4A3), CAM-B3LYP-6-311G* (Fig. 4A4), and TDHF/TZVP (Fig. 4A5) levels. Particularly, S_1 and S_2 states are mainly characterized by the $3 \rightarrow 3$ LE and $2 \rightarrow 2$ LE transitions, respectively. All three levels predict the same energy transfer mechanism and the CT states are not involved at all due to their high energies. By simply increasing r_1 distance, S_1 and S_2 cross to each other and the nonadiabatic decay takes place at this S_1/S_2 conical intersection. Because the S_1/S_2 crossing exists at the shorter distance ($r_1 = 1.26$ Ang) at the TDHF level, the even faster nonadiabatic decay and energy-transfer dynamics should be predicted. Roitberg and coworkers also suggested a similar mechanism by their nonadiabatic dynamics simulation at the semi-empirical AM1/CIS level.^[11] They concluded that the r_1 stretching motion

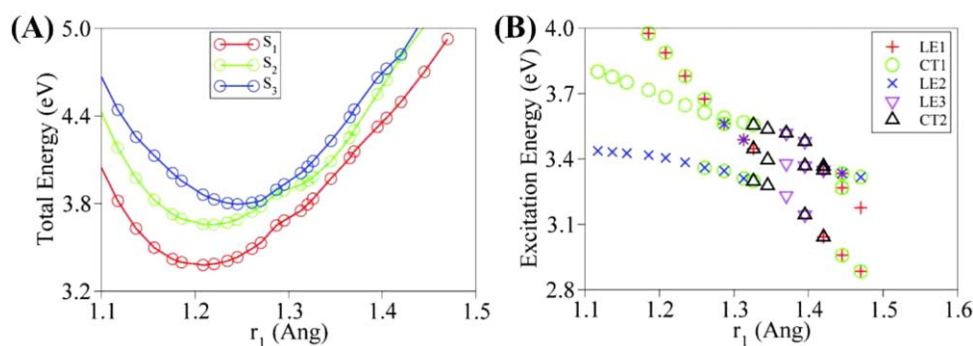


Figure 6. The results at DFT/MRCI level: A) The PES as the function of r_1 (S_1 : red, S_2 : green, S_3 : blue, S_4 : magenta, S_5 : brown, S_6 : turquoise); B) The dependence of all electronic transitions on r_1 and excitation energies (LE1: plus, CT1: circle, LE2: x, LE3: triangle down, CT2: triangle up). [Color figure can be viewed in the online issue, which is available at wileyonlinelibrary.com.]

creates a S_1/S_2 conical intersection responsible for the energy transfer, since most $S_2 \rightarrow S_1$ hops take place around 1.22–1.24 Ång. Thus, their AM1/CIS PES should be very close to the PESS at the TDHF level, as well as qualitatively similar to those at the BH&HLYP and CAM-B3LYP levels.

All above theoretical levels except TDDFT/B3LYP predict the importance of the r_1 stretching motion in the excited-state energy transfer process. This process is not governed by the r_2 and r_3 stretching motions, as well as the A'' electronic states. Here, we only show the results at the SCS-ADC(2) level (Fig. 5) and keep other results in SI (Figure S13-S16).

The PESs derived from the above methods do not provide very consistent energy-transfer mechanisms. As a further comparison, we carried out the subsequent DFT/MRCI calculations. At DFT/MRCI level, (Fig. 6), one CT state (S_2) lies between the $2 \rightarrow 2$ LE state (S_1) and the lowest $3 \rightarrow 3$ LE state (S_3). The S_2/S_3 conical intersection and the S_1/S_2 strong mixing were observed at 1.29 and 1.34 Ång, respectively. Therefore, DFT/MRCI suggests the direct 2-ring \rightarrow 3-ring energy transfer funnel with r_1 stretching motion while the lowest CT state may be weakly involved. However, the direct decay should be very efficient since the crossing near 1.34 Ång is characterized by the strong mixture of LE1 and LE2. Therefore, comparison of the DFT/MRCI and BH&HLYP results shows that the energy transfer mechanism is almost the same, just except the pulled down CT state at the DFT/MRCI level.

As a summary, the SCS-ADC(2) calculations suggest a more complex channel involving several excited states while TDDFT (TDDFT/BH&HLYP, TDDFT/CAM-B3LYP, TDHF) and DFT/MRCI suggest a relatively direct 2-ring \rightarrow 3-ring energy transfer channel. Furthermore, DFT/MRCI drives a relative consistent conclusion with BH&HLYP. All above levels except TDDFT/B3LYP predict that the stretching motion of r_1 plays a dominant role for the excited-state energy transfer process. As a contrast, the other two ethynylene bond distances r_2 and r_3 seem to be irrelevant. Although the A'' excited states may cross to the A' states, these crossings are in the high energy region. This indicates that the direct decay mechanism and reactive coordinate suggested by Roitberg and coworkers at AM1/CIS level^[11] may still be reasonable from a qualitative point of view at more accurate levels. However, the precise

and detailed mechanism is still difficult to be achieved due to various results at different theoretical levels.

Discussions

As well known, the excited-state calculation results are highly dependent on the method selections.^[37,38,54,77] The precise reaction mechanism of photoinduced processes is often not easily determined although the careful benchmark calculations are performed.^[54] Quite commonly it is very difficult to reach a consistent conclusion even for small organic systems. The similar problem happens in the current system as well.

Although the TDDFT approaches are assumed as useful and easy tools in the description of valence excited states, they strongly underestimate the energy of the CT states.^[32,53,54] The employment of hybrid functionals with higher or long-range corrected HF exchanges gives better results for some well-known examples while in other cases this treatment only show the tendency to shift the CT excitation into the higher energy domain. For instance, in this system, the B3LYP gives two CT states lower than the $2 \rightarrow 2$ LE state while the BH&HLYP and CAM-B3LYP functionals show the reversed situation. For some excited states including both LE and CT excitations, the CT components decrease when more HF exchanges are used. The contributions of the long-range CT excitations are also suppressed even for the CT states themselves when the higher HF exchange is included. The TDHF method, as discussed in previous work, tends to overestimate the CT excitations.^[54]

As shown in Figure 7, the vertical energies of bright $3 \rightarrow 3$ LE state are shift to high energy domain, from ~ 3.4 eV (B3LYP and DFT/MRCI), to ~ 3.9 eV (BH&HLYP and CAM-B3LYP), furthermore to ~ 4.3 eV (SCS-ADC(2)) and ~ 4.4 eV (TDHF). The energy differences between the bright $2 \rightarrow 2$ LE and lowest $3 \rightarrow 3$ LE state are ~ 0.8 eV (B3LYP), ~ 0.6 eV (BH&HLYP, CAM-B3LYP, SCS-ADC(2)), and ~ 0.5 eV (TDHF and DFT/MRCI). In the experimental results,^[16] the vertical energy of bright $3 \rightarrow 3$ LE state is 3.5 eV and the energy difference between the bright $2 \rightarrow 2$ LE and lowest $3 \rightarrow 3$ LE state is 0.5 eV. As a propagation method without the deficiency of the CT problem,^[62] ADC(2) sometimes serves as a benchmark method for middle-sized

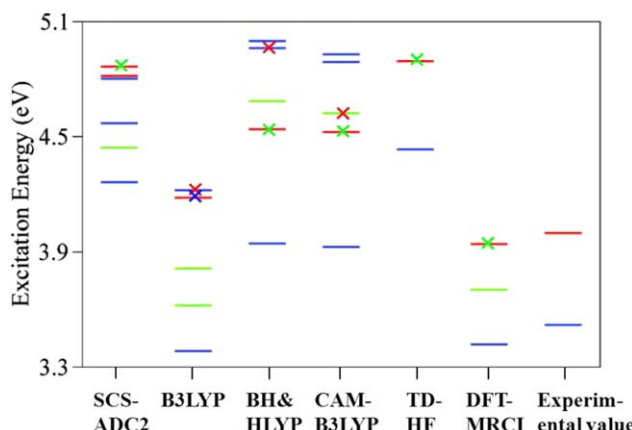


Figure 7. Low-lying excited states with different computational levels and experimental data. The blue, green, and red colors represent the $3 \rightarrow 3$ LE transition, the CT ($2 \rightarrow 3$, $3 \rightarrow 2$) transitions, and the $2 \rightarrow 2$ LE, respectively. The solid lines and crosses denote the major and secondary electronic characters of each excited state.

systems that are beyond the limit of other higher-level *ab initio* correlated methods (such as CASPT2^[38,91,92]). This approach seems to become popular in recent years, see Refs. [93] and [94]. However, in this system the ADC(2) method predicts completely different PES and thus no consistent reaction mechanisms can be derived. For instance, all other levels suggest that the second dark $3 \rightarrow 3$ LE state is higher than the first bright $2 \rightarrow 2$ LE state while the SCS-ADC(2) gives the reversed answers. In this sense, the way to use SCS-ADC(2) data as the benchmark to determine the reasonable percentage of the HF exchange in TDDFT seems not to be a suitable choice for this system. As a comparison, the data at the DFT/MRCI level seems to be consistent with the experimental result.^[16] In addition, previous benchmark calculations recommend that the DFT/MRCI provides very reliable results on many organic systems for both the valence and CT excitations. Owing to these reasons, the DFT/MRCI may be served as the suitable benchmark method to examine the outcomes of TDDFT. In this sense, the 2-ring \rightarrow 3-ring intramolecular energy transfer should be rather directly driven by the crossing between two states characterized by these two electronic characters.

Overall, the inconsistency in this work exactly reflects the dilemma in the electronic-structure calculations of molecular excited states.^[95] Therefore, the development of novel methods and improvement of available methods represent the great challenging for the future. For this system, the results are sometimes highly sensitive to the method selection; however, the quantitative consistent conclusion can be made after very careful calculations. For example, all methods predicted that the elongation of r_1 results in the orbital variation. The frontier orbital energies as the function of r_1 at different levels are shown in Figure S17 of SI. With the increasing of r_1 , HOMO and HOMO-1 (as well as LUMO and LUMO+1) start to be close to each other and form the avoided crossing. During this process, the MOs undergo the localization \rightarrow delocalization \rightarrow localization variation. We took TDDFT/BH&HLYP result as a typical example for illustration (Fig. 8) as all levels of theories give the similar picture. In principle, two highest occupied orbitals

(HOMO-1 and HOMO) can be formed by the linear combination of two occupied localized orbitals (named as OLO2 and OLO3) localized in the 2-ring and 3-ring units, respectively. Because of different conjugation lengths of two fragments, the OLO2 energy should be much lower than the OLO3 energy at the FC region. The OLO2-OLO3 energy difference is much larger than their electronic interaction and the final MOs are still localized in each unit. Thus, the resulted HOMO and HOMO-1 are basically equivalent to the OLO3 and OLO2, respectively. When the r_1 distance becomes longer, the energy of OLO3 should remain almost unchanged because its energy and density are not relevant to r_1 . However, the elongation of the r_1 distance should reduce the B1-B3 electronic interactions. As a result, the energy of OLO2 should increase. In the vicinity of $r_1 = 1.37$ Å, the energies of OLO2 and OLO3 become similar. In this case, their electronic interactions play a dominant role and the overall MOs become the linear (symmetrical or anti-symmetrical) combinations of two local orbitals. Thus, the completed orbital delocalization is observed for both HOMO and HOMO-1. The further elongation of the r_1 bond distance again enhances the energy difference of OLO2 and OLO3. This results in the localization of HOMO and

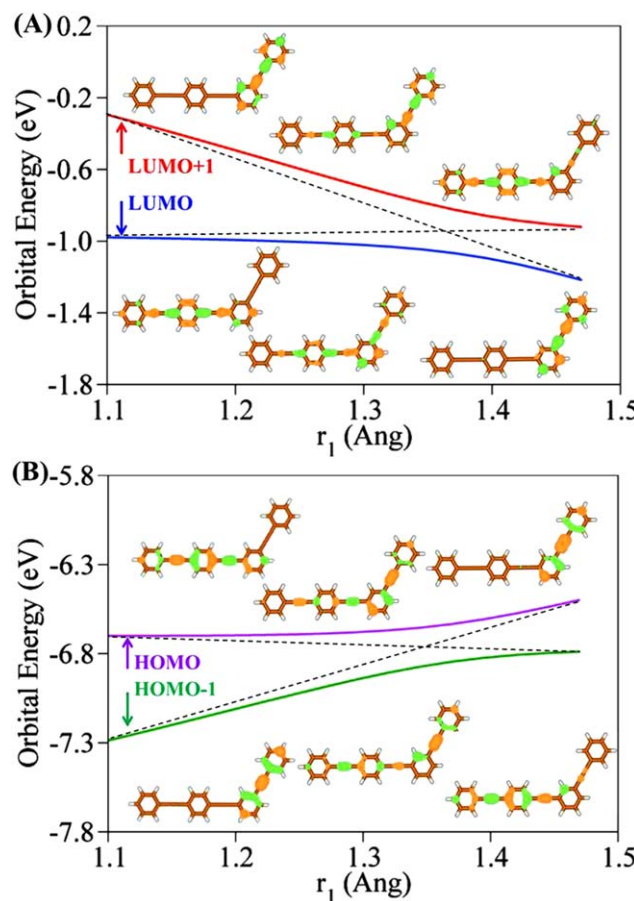


Figure 8. The four frontier orbital (HOMO-1, HOMO, LUMO, and LUMO+1) energies as the function of r_1 at the TDDFT/BH&HLYP level. The corresponding orbitals are plotted at r_1 1.20, 1.37, and 1.47 Å. [Color figure can be viewed in the online issue, which is available at wileyonlinelibrary.com.]

HOMO-1 again while the HOMO becomes OLO2 now. The similar two-level model can be used to understand the behavior of LUMO and LUMO-1. Near 1.37 Å, we expected that 2 → 2 and 3 → 3 excitation should have similar transition energies due to the highly mixed character of four frontier MOs. This explains why the state crossing and mixing are observed in the longer r_1 distance. In another word, the mixing between localized orbitals should play a key role to form the relevant conical intersections (or avoided crossings) governing the 2-ring → 3-ring excited state energy transfer. This also clarifies why r_1 is assumed as the reaction coordinate through electronic-structure calculations. In this sense, we expect that the result of nonadiabatic dynamics at the AM1/CIS level by Roitberg et al. should be qualitatively reasonable, although these high-level calculations somehow do not reach a very consistent and decisive conclusion. Therefore, the more precise understanding of excited states of such systems still require the developments of novel quantum chemistry methods and the progress of computational ability. Certainly, the nonadiabatic dynamics at high-level methods should also represent a challenging task in the future.

Conclusions

In this article, we performed systematic benchmark calculations with different electronic-structure methods to understand the optoelectronic characters of PE dendrimers. Several methods, SCS-ADC(2), TDHF, TDDFT with B3LYP, BH&HLYP and CAM-B3LYP functionals, and DFT/MRCI were used. The vertical excitation energies and the electronic characters of excited states were discussed in details. At the FC region, the electronic transitions were analyzed using both orbital picture and transition density. By considering the one-electron transition density matrix within Löwdin orbitals, we successfully distinguished the intrinsic features of each state, as well as directly obtained the contributions of all intraunit and interunit excitations. The PESs along three different coordinates (ethynylene bond r_1 , r_2 , and r_3) were constructed.

Although various results are obtained in different levels, the energy transfer mechanism derived from DFT/MRCI level is consistent with that of TDDFT/BH&HLYP if we simply shift down the CT state obtained at the BH&HLYP level. Although the TDDFT method (BH&HLYP and CAM-B3LYP) and the TDHF theory suggest the similar picture, namely the direct 2-ring → 3-ring energy transfer via the ultrafast $S_2 \rightarrow S_1$ decay, the SCS-ADC(2) seems to recommend a more complex process involving many intermediated electronic states. This analysis identifies that result from the TDDFT/BH&HLYP calculation is close to that of DFT/MRCI. And DFT/MRCI shows good agreement with experimental vertical excitation energies.

Here, some qualitative picture may be also derived. When the ethynylene bond distance r_1 becomes longer, the frontier orbitals become delocalized and such orbital variation should be relevant to the 2-ring → 3-ring energy transfer. As a contrast, the exciton energy transfer is not governed by the stretching motions of triple bonds in the 3-ring unit (r_2 and r_3) and the A'' excited states. The current analysis will not only

provide a solid basis for the further investigation but also show the dilemma of excited-states calculations. In this situation, the precise understanding of optical-electronic properties of PE dendrimers and other similar systems requires the development of the novel electronic-structure theories, as well as the treatment of nonadiabatic dynamics at more accurate level of theories.

Acknowledgments

The authors thank Supercomputing Center, Computer Network Information Center (Beijing), CAS and the Super Computational Center of CAS-QIBEBT for computational resources and software. The authors also thank the support by Key Lab of Nanodevices and Nanoapplications (14HZ03), Suzhou Institute of Nano-Tech and Nano-Bionics, CAS.

Keywords: tree-like conjugated molecules · spin-component scaling modification ADC(2) (SCS-ADC(2)) · TDDFT · DFT/MRCI · local excitation and charge-transfer excitation · transition density matrix

How to cite this article: J. Huang, L. Du, D. Hu, Z. Lan. *J. Comput. Chem.* **2015**, *36*, 151–163. DOI: 10.1002/jcc.23778

Additional Supporting Information may be found in the online version of this article.

- [1] A. C. Benniston, A. Harriman, *Mater. Today* **2008**, *11*, 26.
- [2] N. S. Lewis, D. G. Nocera, *Proc. Natl. Acad. Sci. U.S.A.* **2006**, *103*, 15729.
- [3] D. Möbius, H. Kuhn, *J. Appl. Phys.* **1988**, *64*, 5138.
- [4] S. F. Swallen, R. Kopelman, J. S. Moore, C. Devadoss, *J. Mol. Struct.* **1999**, *485*, 585.
- [5] M. R. Shortreed, S. F. Swallen, Z. Y. Shi, W. H. Tan, Z. F. Xu, C. Devadoss, J. S. Moore, R. Kopelman, *J. Phys. Chem. B* **1997**, *101*, 6318.
- [6] S. F. Swallen, Z. G. Zhu, J. S. Moore, R. Kopelman, *J. Phys. Chem. B* **2000**, *104*, 3988.
- [7] Z. F. Xu, M. Kahr, K. L. Walker, C. L. Wilkins, J. S. Moore, *J. Am. Chem. Soc.* **1994**, *116*, 4537.
- [8] R. Kopelman, M. Shortreed, Z. Y. Shi, W. H. Tan, Z. F. Xu, J. S. Moore, A. BarHaim, J. Klafter, *Phys. Rev. Lett.* **1997**, *78*, 1239.
- [9] C. Wu, S. V. Malinin, S. Tretiak, V. Y. Chernyak, *Nat. Phys.* **2006**, *2*, 631.
- [10] C. Devadoss, P. Bharathi, J. S. Moore, *J. Am. Chem. Soc.* **1996**, *118*, 9635.
- [11] S. Fernandez-Alberti, V. D. Kleiman, S. Tretiak, A. E. Roitberg, *J. Phys. Chem. A* **2009**, *113*, 7535.
- [12] J. M. J. Fréchet, *Science* **1994**, *263*, 1710.
- [13] S. Mukamel, *Nature* **1997**, *388*, 425.
- [14] J. L. Palma, E. Atas, L. Hardison, T. B. Marder, J. C. Collings, A. Beeby, J. S. Melinger, J. L. Krause, V. D. Kleiman, A. E. Roitberg, *J. Phys. Chem. C* **2010**, *114*, 20702.
- [15] D. Rana, G. Gangopadhyay, *Chem. Phys. Lett.* **2001**, *334*, 314.
- [16] V. D. Kleiman, J. S. Melinger, D. McMorrow, *J. Phys. Chem. B* **2001**, *105*, 5595.
- [17] M. I. Ranasinghe, M. W. Hager, C. B. Gorman, T. Goodson, *J. Phys. Chem. B* **2004**, *108*, 8543.
- [18] D. G. Kuroda, C. P. Singh, Z. Peng, V. D. Kleiman, *Science* **2009**, *326*, 263.
- [19] W. Ortiz, B. P. Krueger, V. D. Kleiman, J. L. Krause, A. E. Roitberg, *J. Phys. Chem. B* **2005**, *109*, 11512.
- [20] A. BarHaim, J. Klafter, R. Kopelman, *J. Am. Chem. Soc.* **1997**, *119*, 6197.
- [21] S. Tretiak, V. Chernyak, S. Mukamel, *J. Phys. Chem. B* **1998**, *102*, 3310.
- [22] T. Minami, S. Tretiak, V. Chernyak, S. Mukamel, *J. Lumin.* **2000**, *87*–89, 115.

- [23] T. Tada, D. Nozaki, M. Kondo, K. Yoshizawa, *J. Phys. Chem. B* **2003**, *107*, 14204.
- [24] J. C. Kirkwood, C. Scheurer, V. Chernyak, S. Mukamel, *J. Chem. Phys.* **2001**, *114*, 2419.
- [25] A. Tortschanoff, S. Mukamel, *J. Phys. Chem. A* **2002**, *106*, 7521.
- [26] S. Tretiak, S. Mukamel, *Chem. Rev.* **2002**, *102*, 3171.
- [27] A. L. Thompson, K. M. Gaab, J. Xu, C. J. Bardeen, T. J. Martínez, *J. Phys. Chem. A* **2004**, *108*, 671.
- [28] K. M. Gaab, A. L. Thompson, J. Xu, T. J. Martínez, C. J. Bardeen, *J. Am. Chem. Soc.* **2003**, *125*, 9288.
- [29] S. Fernandez-Alberti, V. D. Kleiman, S. Tretiak, A. E. Roitberg, *J. Phys. Lett.* **2010**, *1*, 2699.
- [30] M. A. Soler, A. E. Roitberg, T. Neson, S. Tretiak, S. Fernandez-Alberti, *J. Phys. Chem. A* **2012**, *116*, 9802.
- [31] S. Fernandez-Alberti, A. E. Roitberg, V. D. Kleiman, T. Nelson, S. Tretiak, *J. Chem. Phys.* **2012**, *137*, 22A526.
- [32] L. Gonzalez, D. Escudero, L. Serrano-Andres, *ChemPhysChem* **2012**, *13*, 28.
- [33] F. Plasser, M. Barbatti, A. J. A. Aquino, H. Lischka, *Theor. Chem. Acc.* **2012**, *131*, 1073.
- [34] S. Grimme, M. Waletzke, *J. Chem. Phys.* **1999**, *111*, 5645.
- [35] F. Réal, V. Vallet, C. Marian, U. Wahlgren, *J. Chem. Phys.* **2007**, *127*, 214302.
- [36] D. Escudero, W. Thiel, *J. Chem. Phys.* **2014**, *140*, 194105.
- [37] K. Sen, R. Crespo-Otero, O. Weingart, W. Thiel, M. Barbatti, *J. Chem. Theory Comput.* **2013**, *9*, 533.
- [38] M. R. Silva-Junior, M. Schreiber, S. P. A. Sauer, W. Thiel, *J. Chem. Phys.* **2008**, *129*, 104103.
- [39] S. Grimme, *Chem. Phys. Lett.* **1996**, *259*, 128.
- [40] C. M. Marian, N. Gilka, *J. Chem. Theory Comput.* **2008**, *4*, 1501.
- [41] D. J. Rowe, *Rev. Mod. Phys.* **1968**, *40*, 153.
- [42] J. Rose, T. I. Shibuya, V. McKoy, *J. Chem. Phys.* **1973**, *58*, 74.
- [43] M. F. Herman, K. F. Freed, D. L. Yeager, Analysis and Evaluation of Ionization Potentials, Electron Affinities, and Excitation Energies by the Equations of Motion—Green's Function Method; Advances in Chemical Physics; Vol. 48; Wiley: New York, **2007**; pp. 1–69.
- [44] M. Schreiber, M. R. Silva-Junior, S. P. A. Sauer, W. Thiel, *J. Chem. Phys.* **2008**, *128*, 134110.
- [45] I. Alata, R. Omidyan, M. Broquier, C. Dedonder, O. Dopfer, C. Jouvet, *Phys. Chem. Chem. Phys.* **2010**, *12*, 14456.
- [46] A. B. Trofimov, G. Stelter, J. Schirmer, *J. Chem. Phys.* **1999**, *111*, 9982.
- [47] P. H. P. Harbach, M. Wormit, A. Dreuw, *J. Chem. Phys.* **2014**, *141*, 064113.
- [48] A. B. Trofimov, J. Schirmer, *J. Phys. B: At., Mol. Opt. Phys.* **1995**, *28*, 2299.
- [49] A. J. A. Aquino, D. Nachtigallova, P. Hobza, D. G. Truhlar, C. Hättig, H. Lischka, *J. Comput. Chem.* **2011**, *32*, 1217.
- [50] I. L. Rusaková, L. B. Krivdin, Y. Y. Rusakov, A. B. Trofimov, *J. Chem. Phys.* **2012**, *137*, 044119.
- [51] D. Rappoport, F. Furche, *J. Chem. Phys.* **2005**, *122*, 064105.
- [52] R. Bauernschmitt, R. Ahlrichs, *Chem. Phys. Lett.* **1996**, *256*, 454.
- [53] A. Dreuw, M. Head-Gordon, *Chem. Rev.* **2005**, *105*, 4009.
- [54] W. Liu, V. Settels, P. H. P. Harbach, A. Dreuw, R. F. Fink, B. Engels, *J. Comput. Chem.* **2011**, *32*, 1971.
- [55] J. L. Bredas, D. Beljonne, V. Coropceanu, J. Cornil, *Chem. Rev.* **2004**, *104*, 4971.
- [56] T. M. Clarke, J. R. Durrant, *Chem. Rev.* **2010**, *110*, 6736.
- [57] V. Settels, W. Liu, J. Pflaum, R. F. Fink, B. Engels, *J. Comput. Chem.* **2012**, *33*, 1544.
- [58] S. Tretiak, A. Saxena, R. L. Martin, A. R. Bishop, *Phys. Rev. Lett.* **2002**, *89*, 097402.
- [59] A. V. Luzanov, O. V. Prezhdo, *Int. J. Quantum Chem.* **2005**, *102*, 582.
- [60] A. V. Luzanov, O. A. Zhikol, *Int. J. Quantum Chem.* **2010**, *110*, 902.
- [61] F. Plasser, H. Lischka, *J. Chem. Theory Comput.* **2012**, *8*, 2777.
- [62] F. Plasser, A. J. A. Aquino, W. L. Hase, H. Lischka, *J. Phys. Chem. A* **2012**, *116*, 11151.
- [63] F. Plasser, S. A. Bappler, M. Wormit, A. Dreuw, *J. Chem. Phys.* **2014**, *141*, 024107.
- [64] F. Plasser, M. Wormit, A. Dreuw, *J. Chem. Phys.* **2014**, *141*, 024106.
- [65] F. Wu, W. Liu, Y. Zhang, Z. Li, *J. Chem. Theory Comput.* **2011**, *7*, 3643.
- [66] A. A. Voityuk, *J. Chem. Phys.* **2014**, *140*, 244117.
- [67] A. Schubert, V. Settels, W. Liu, F. Würthner, C. Meier, R. F. Fink, S. Schindlbeck, S. Lochbrunner, B. Engels, V. Engel, *J. Phys. Lett.* **2013**, *4*, 792.
- [68] W. Liu, Exciton Coupling in Valence and Core Excited Aggregates of π -Conjugated Molecules, Ph.D. Thesis, Dissertation zur Erlangung des naturwissenschaftlichen Doktorgrades der Julius-Maximilians-Universität Würzburg, **2011**.
- [69] W. J. D. Beenken, T. Pullerits, *J. Phys. Chem. B* **2004**, *108*, 6164.
- [70] R. L. Martin, *J. Chem. Phys.* **2003**, *118*, 4775.
- [71] J. Auerswald, B. Engels, I. Fischer, T. Gerlich, J. Herterich, A. Krueger, M. Lang, H. C. Schmitt, C. Schon, C. Walter, *Phys. Chem. Chem. Phys.* **2013**, *15*, 8151.
- [72] Y. Yi, V. Coropceanu, J. L. Bredas, *J. Am. Chem. Soc.* **2009**, *131*, 15777.
- [73] D. Fazzi, M. Cairoli, C. Castiglioni, *J. Am. Chem. Soc.* **2011**, *133*, 19056.
- [74] G. Grancini, D. Polli, D. Fazzi, J. Cabanillas-Gonzalez, G. Cerullo, G. Lanzani, *J. Phys. Lett.* **2011**, *2*, 1099.
- [75] T. Minami, M. Nakano, F. Castet, *J. Phys. Lett.* **2011**, *2*, 1725.
- [76] J. Olsen, H. J. A. Jensen, P. Jorgensen, *J. Comput. Phys.* **1988**, *74*, 265.
- [77] S. S. Leang, F. Zahariev, M. S. Gordon, *J. Chem. Phys.* **2012**, *136*, 104101.
- [78] P. A. M. Dirac, *Proc. R. Soc. A* **1929**, *123*, 714.
- [79] J. C. Slater, *Phys. Rev.* **1951**, *81*, 385.
- [80] C. T. Lee, W. T. Yang, R. G. Parr, *Phys. Rev. B* **1988**, *37*, 785.
- [81] A. D. Becke, *Phys. Rev. A* **1988**, *38*, 3098.
- [82] S. H. Vosko, L. Wilk, M. Nusair, *Cancer. J. Phys.* **1980**, *58*, 1200.
- [83] A. D. Becke, *J. Chem. Phys.* **1993**, *98*, 1372.
- [84] T. Yanai, D. P. Tew, N. C. Handy, *Chem. Phys. Lett.* **2004**, *393*, 51.
- [85] A. Hellweg, S. A. Gruen, C. Haettig, *Phys. Chem. Chem. Phys.* **2008**, *10*, 4119.
- [86] J. H. Starcke, M. Wormit, J. Schirmer, A. Dreuw, *Chem. Phys.* **2006**, *329*, 39.
- [87] R. Ahlrichs, M. Bär, M. Häser, H. Horn, C. Kölmel, *Chem. Phys. Lett.* **1989**, *162*, 165.
- [88] M. J. Frisch, J. A. Pople, J. S. Binkley, *J. Chem. Phys.* **1984**, *80*, 3265.
- [89] I. Mayer, *Chem. Phys. Lett.* **1983**, *97*, 270.
- [90] P. O. Löwdin, In Advances in Quantum Chemistry; P. O. Löwdin, Ed.; Vol. 5; Academic Press: New York, **1970**; pp. 185–199.
- [91] G. Ghigo, B. O. Roos, P. A. Malmqvist, *Chem. Phys. Lett.* **2004**, *396*, 142.
- [92] M. Schreiber, M. R. J. Silva, S. P. A. Sauer, W. Thiel, *J. Chem. Phys.* **2008**, *128*, 134110.
- [93] S. Yamazaki, A. L. Sobolewski, W. Domcke, *Phys. Chem. Chem. Phys.* **2009**, *11*, 10165.
- [94] A. N. Panda, F. Plasser, A. J. A. Aquino, I. Burghardt, H. Lischka, *J. Phys. Chem. A* **2013**, *117*, 2181.
- [95] M. Schreiber, M. Barbatti, S. Zilberg, H. Lischka, L. González, *J. Phys. Chem. A* **2006**, *111*, 238.

Received: 27 May 2014

Revised: 5 September 2014

Accepted: 13 October 2014

Published online on 21 November 2014